ISBN: 978-3-95450-257-8 ISSN: 2222-5692 doi:10.18429/JACoW-ECRIS2024-THA3

WAVEGUIDE DC BREAKS WITH OPTIMIZED IMPEDANCE MATCHING NETWORKS*

M. Kireeff Covo†, J. Benitez, D. Todd, J. Cruz Duran, P. Bloemhard, M. Johnson, J. Garcia, B. Ninemire, D. Xie, and L. Phair, Lawrence Berkeley National Laboratory, CA, USA

Abstract

A custom 18 GHz waveguide DC break with a built-in impedance matching network, consisting of two inductive irises adjacent to a capacitive gap assembled around a quartz disk, was built for Versatile ECR for Nuclear Science (VENUS) ion source and simulated using the ANSYS High Frequency Structure Simulator, a finite element analysis tool. The DC break effectively doubled the RF power available for plasma production at the secondary frequency of 18 GHz while maintaining a DC isolation of 32 kV. Measurements of the forward and reflected power coefficients, performed with a network analyzer, showed excellent agreement with the simulations [1]. Additionally, an extended study was conducted to tailor the frequencies of 28, 35, and 45 GHz using WR-34, WR-28, and WR-22 waveguides with built-in impedance matching networks, aiming to predict performance for our upcoming 4th generation low-power, multi-frequency operation of the MARS-D ion source.

INTRODUCTION

The Versatile Electron Cyclotron Resonance (VENUS) ion source, developed at Lawrence Berkeley National Laboratory's 88-Inch Cyclotron [2], operates at frequencies of 28 GHz and 18 GHz. It utilizes a superconducting magnet system to generate a strong, well-defined magnetic field for confinement, creating two enclosed regions for plasma heating and enabling the production of ion beams with high charge states and intensities.

Since the VENUS ion source operates on a high-voltage platform meanwhile the RF system is at ground potential, a waveguide HV DC break is required to maintain isolation while allowing RF signals to pass with minimal microwave leakage and insertion losses [3].

DC breaks can be mainly categorized into two types. One common type is the choke flange [4–6], which creates a gap in the waveguide using dielectric materials to achieve isolation. Another type is the multi-layer DC break [7, 8], which uses multiple layers of insulating materials between sections of metal, enhancing the overall dielectric strength and reducing RF leakage. Some advanced designs use innovative techniques, such as a lattice structure made of dielectric materials [9] or tapered waveguide transitions combined with low-loss dielectrics [10]. To further enhance RF power delivery and compensate for waveguide mismatches, tuners equipped with screws, posts, or stubs are often used just before the DC break, improving impedance matching and maximizing power transfer to the plasma [11–13].

WAVEGUIDE DC BREAK

The DC break is constructed using two open-ended copper sections that conform to the WR-62 waveguide's dimensions, with a width of 15.8 mm and a height of 7.9 mm. This break includes a gap within the waveguide filled by a fused quartz disk, measuring 100 mm in diameter and 1 mm in thickness [14]. The quartz, known for its excellent thermal properties and high dielectric strength, allows the system to withstand up to 32 kV DC, furthermore, its low dielectric constant of 3.9 and very low dielectric loss tangent of less than 1×10^{-3} ensure minimal RF energy loss, calculated to be about 0.003 dB. This results in the primary losses being due to RF leakage, calculated by subtracting the total transmitted and reflected power from 100 %.

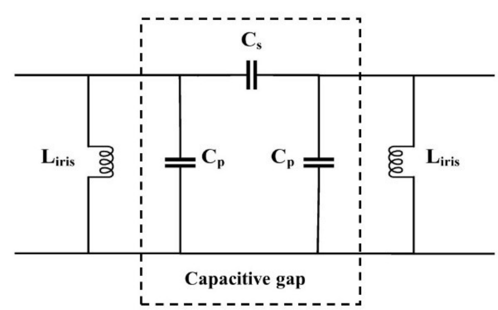

Figure 1: Waveguide DC break equivalent circuit.

To address impedance mismatches caused by the gap, the design incorporates two symmetrical inductive matching irises [15], each 1.85 mm thick, positioned adjacent to the gap. As illustrated in Fig. 1, the gap introduces lumped capacitance C_p due to fringing fields at the open-ended waveguides and series capacitive coupling C_s across the gap, leading to impedance mismatch. The irises generate lumped shunt inductances L_{iris}, which compensates for the lumped shunt capacitances C_p, effectively creating a band-pass filter centered around the desired frequency. Additionally, the waveguide apertures near the gap are expanded to form a

* Work supported by the Director, Office of Science, Office of Nuclear Physics, Division of Nuclear Physics, U.S. Department of Energy under Contract No. DE-AC02-05CH11231 and by the U.S. Army Program Executive Office, Simulation, Training and Instrumentation (PEO STRI), Test Resource Management Center (TRMC) Test and Evalua-tion/Science & Technology (T&E/S&T) Program. These projects are funded by the T&E/S&T Program through the U.S. Army Program Executive Office for Simulation, Training, and Instrumentation (PEO STRI) Instrumentation Management Office (IMO). Disclaimer: Any opinions, findings, and conclusions, or recommendations expressed in this material are those of the author(s) and do not necessarily reflect the views of the Test Resource Management Center (TRMC) Test and Evaluation/Science & Technology (T&E/S&T) Program and/or the Program Executive Office for Simulation, Training & Instrumentation (PEO STRI).
† mkireeffcovo@lbl.gov

ISBN: 978-3-95450-257-8 ISSN: 2222-5692 doi:10.18429/JACoW-ECRIS2024-THA3

circular surface with a diameter of 67.06 mm, resulting in a series capacitance of approximately 1207 pF at 18 GHz. This setup helps reduce reflections and minimize power loss.

Using Marcuvitz's formula, as shown in Eq. (1), for estimating inductive reactance [16], the design achieves an inductive reactance of 485.33 Ω, equivalent to an inductance of 4.29 nH, by choosing a window width of 7.87 mm and an iris width of 3.96 mm.

$$\frac{X_L}{Z_0} \approx \frac{a}{\lambda_g}\cot^2\frac{\pi d'}{a}\left[1+\frac{2}{3}\left(\frac{\pi d'}{\lambda}\right)^2\right], \quad \frac{d'}{a} \ll 1\,, \tag{1}$$

where X_L represents the inductive reactance, Z_0 is the characteristic impedance of the waveguide, a is the width of the waveguide, λ_g is the guide wavelength, d' is the effective width of the iris or discontinuity within the waveguide, and λ is the free-space wavelength.

The resonance frequency f_r can be calculated with the L_{iris} lumped inductance resultant from the iris in parallel with the C_p lumped parallel capacitance resultant from the open-ended waveguide, obtained from Eq. (2):

$$f_r = \frac{1}{2\pi\sqrt{L_{iris}C_p}}\,. \tag{2}$$

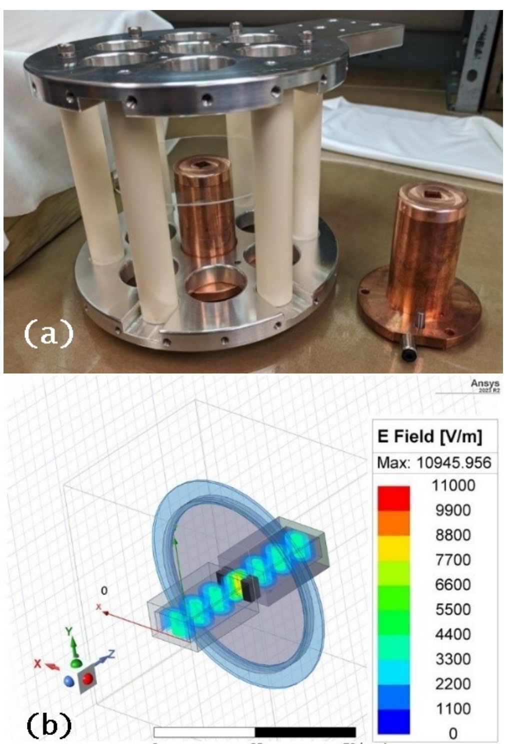

Figure 2: Waveguide DC break: (a) hardware with an inductive iris impedance matching network. One open ended waveguide section is placed aside. (b) HFSS simulated magnitude of the electric field for the TE10 mode.

Adjusting the iris width allows fine-tuning of the resonance frequency by changing L_{iris}. This design ensures efficient RF transmission and minimizes losses, validated through simulations and experimental measurements to optimize the device for use at the klystron frequency of 18 GHz.

HARDWARE

The hardware shown in Fig. 2(a) consists of a WR-62 waveguide within a copper cylindrical structure, featuring a gap for series capacitance, nitrogen gas injection for a non-reactive environment, and ceramic standoffs securing the components, all encased in a metallic shield to prevent RF leakage (not shown in the image).

The HFSS [17] 3D model shown in Fig. 2(b) displays the electric field distribution for the TE10 mode at 18 GHz and it is used for simulating RF transport. The mesh was refined to a maximum element length of 5 mm, utilizing broadband adaptive solutions from 11.6 to 18.6 GHz, with the waveguide constructed from a perfect electric conductor.

Figure 3 shows that the resonance frequency is determined by the minimum S_{11} value in the simulation, indicating optimal impedance matching, while the S_{21} parameter measures the efficiency of RF power transmission through the waveguide. Measurements performed with a network analyzer show excellent agreement with the simulation.

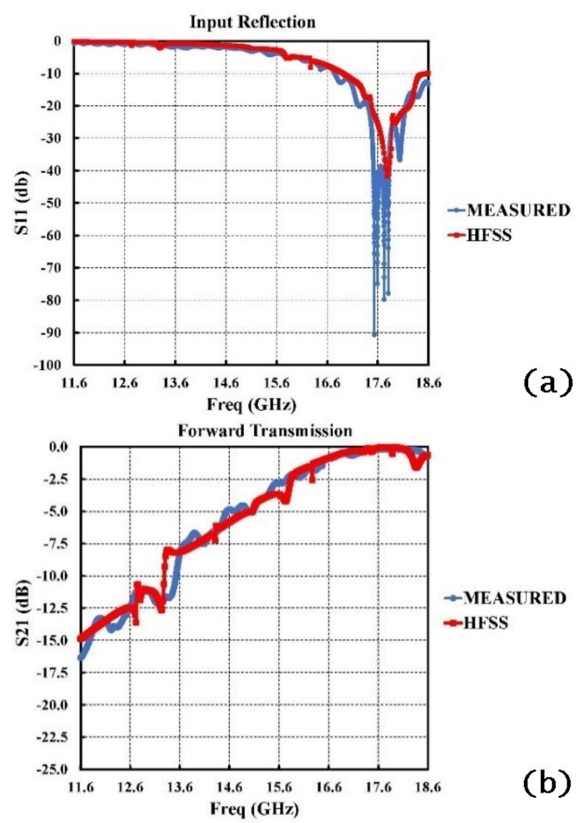

Figure 3: Comparison of S parameters obtained with HFSS simulations and measurements: (a) S_{11} input reflection, (b) S_{22} forward transmission.

The new DC break effectively doubled the RF power available for plasma production at the secondary frequency of 18 GHz while maintaining a DC isolation of 32 kV.

26th Int. Workshop Electron Cyclotron Resonance Ion Sources ECRIS2024, Darmstadt, Germany JACoW Publishing
ISBN: 978-3-95450-257-8 ISSN: 2222-5692 doi:10.18429/JACoW-ECRIS2024-THA3

OPTIMIZATION

To predict performance for our upcoming 4th generation low-power, multi-frequency operation of the MARS-D ion source, an extended study was conducted to tailor the frequencies of 28, 35, and 45 GHz using WR-34, WR-28, and WR-22 waveguides with built-in impedance matching networks, aiming to optimize the HV DC break.

Since MARS-D requires an isolation of 45 kV, a feasibility study was performed with the WR-22 waveguide dimensions. In the simulation, the quartz thickness was gradually increased until it nearly doubled, with the corresponding resonant frequency shown in Fig. 4. As the thickness increased, the resonant frequency f_r decreased due to the increase in shunt capacitance C_p and decrease of the series capacitance C_s. Simultaneously, the insertion loss and the RF leakage also increases.

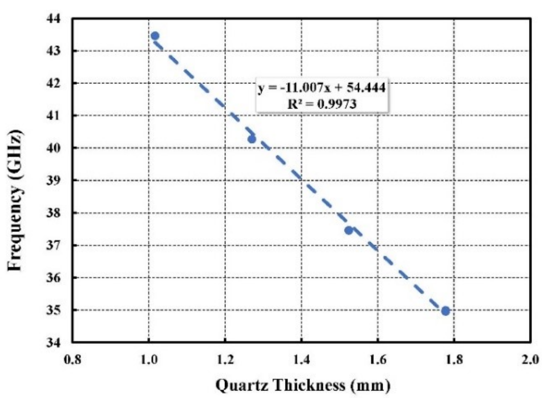

Figure 4: Resonant frequency versus Quartz thickness.

An improved approach to achieve 45 kV isolation is to maintain the quartz thickness of 1 mm and introduce a second gap with additional set of irises, placed at least a couple of wavelengths apart in the waveguide, as shown in the model of Fig. 5. The impedance matching is expected to occur at the same frequency as the first set of irises, with reduced RF leakage and enhanced impedance matching.

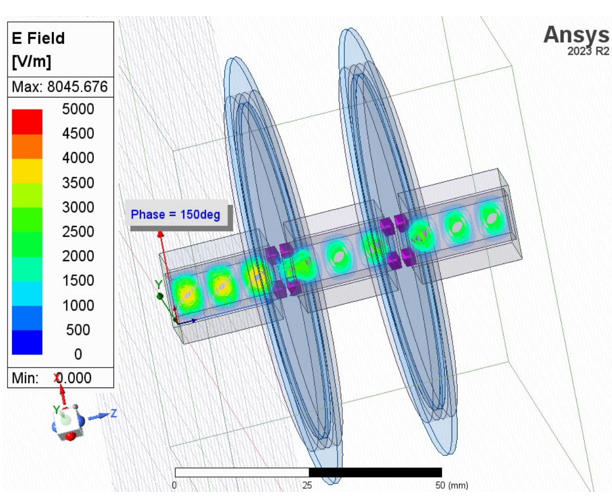

Figure 5: Waveguide DC break with DC isolation of 64 kV.

RESULTS

Table 1 summarizes the required inductive iris aperture W for each waveguide type in the new configuration, ensuring proper impedance matching at the target frequencies.

Table 1: Inductive Iris Aperture

Waveguide	W [mm]	f [GHz]	S_{11} [dB]	S_{21} [dB]
WR34	4.32	28	–39.21	–0.06
WR28	3.20	35	–37.97	–0.04
WR22	2.23	45	–24.30	–0.03

CONCLUSION

The inclusion of inductive irises and quartz-filled capacitive gaps within the waveguide structure has effectively reduced power loss and minimized mismatches at the target frequencies. The successful simulations and measurements underscore the reliability of this design, not only for the VENUS ion source but also as a scalable solution for future MARS-D multi-frequency ion sources.

ACKNOWLEDGEMENTS

The authors thank Brendan P. Ford, Nathaniel Bohm, Erik Line, and Collin Anderson, Shane Blim for their electronics support; Alexander Donoghue, Scott M. Small, Nicholas M. Brickner, Nishi Intwala, Patrick Coleman, and Devin T. Thatcher for their operations support; and Nathan Seidman, Roman Nieto, Donald Bell, and Sixuan Zhong for their mechanical support of the LBNL 88-Inch Cyclotron.

REFERENCES

[1] M. Kireeff Covo *et al.*, "Inductive Iris Impedance Matching Network for a Compact Waveguide DC Break", *IEEE Trans. Microwave Theory Tech.*, early access 2024. doi:10.1109/TMTT.2024.3409470

[2] M. Kireeff Covo *et al.*, "The 88-Inch Cyclotron: A one-stop facility for electronics radiation and detector testing", *Meas.*, vol. 127, pp. 580-587, 2018. doi:10.1016/j.measurement.2017.10.018.M

[3] M.S. Dmitriyev, M.V. Dyakonov, S.A. Tumanov, and M.I. Zhigailova, "DC break design for a 2.45 GHz ECR ion source", in *Proc. 12th Int. Particle Acc. Conf. (IPAC'21)*, São Paulo, Brazil, 2021, pp. 3064-3065. doi:10.18429/JACoW-IPAC2021-WEPAB190

[4] V. Buiculescu and A. Ştefănescu, "Choke flange-like structure for direct connection of cascaded substrate integrated waveguide components", *Electron. Lett.*, vol. 48, no. 21, pp. 1349-1350, Oct. 2012. doi:10.1049/el.2012.2901

[5] A. Misra, I. Chatterjee, and P.Y. Nabhiraj, "Studies on equivalent circuit approach to design waveguide break for 14.45 GHz ECR ion source", in *Proc. IEEE MTT-S Int. Microwave RF Conf. (IMaRC)*, Kolkata, India, 2018, pp. 1-3. doi:10.1109/IMaRC.2018.8877158

ISBN: 978-3-95450-257-8 ISSN: 2222-5692 doi:10.18429/JACoW-ECRIS2024-THA3

[6] M.S. Dmitriev, M.V. Dyakonov, and S.A. Tumanov, "Waveguide Development for a 2.46 GHz Electron Cyclotron Resonance Ion Source", *Phys. Atom. Nuclei*, vol. 85, pp. 1899-1901, 2022. doi:10.1134/S1063778822100143

[7] Y.S. Cho, D.I. Kim, H.S. Kim, K.T. Seol, and H.J. Kwon, "Multi-layered waveguide DC electrical break for the PEFP microwave proton source", *J. Korean Phys. Soc.*, vol. 63, pp. 2085-2088, 2013. doi:10.3938/jkps.63.2085

[8] J. Jo, S.H. Kim, J.-T. Jin, and S.-R. Huh, "Development of waveguide DC break for power transmission at 2.45 GHz and 100-kV insulation", *IEEE Microw. Wireless Compon. Lett.*, vol. 30, no. 4, pp. 339-342, Apr. 2020. doi:10.1109/LMWC.2020.2978639

[9] G.S. Mauro, A. Locatelli, G. Torrisi, L. Celona, C. De Angelis, and G. Sorbello, "Woodpile EBG waveguide as a DC electrical break for microwave ion sources", *Microw. Opt. Technol. Lett.*, vol. 61, pp. 610-614, 2019. doi:10.1002/mop.31628

[10] O. Leonardi, G. Torrisi, G. Sorbello, L. Celona, and S. Gammino, "A compact DC-break for ECR ion source @ 18 GHz", *Microw. Opt. Technol. Lett.*, vol. 60, pp. 3026-3029, 2018. doi:10.1002/mop.31421

[11] L. Celona, G. Ciavola, and S. Gammino, "Study of microwave coupling in electron cyclotron resonance ion sources and microwave ion sources", *Rev. Sci. Instrum.*, vol. 69, no. 2, pp. 1113-1115, Feb. 1998. doi:10.1063/1.1148640

[12] T. Taylor and J.F. Mouris, "An advanced high-current low-emittance dc microwave proton source", *Nucl. Instrum. Methods Phys. Res., Sect. A*, vol. 336, no. 1-2, pp. 1-5, Jan. 1993. doi:10.1016/0168-9002(93)91074-W

[13] F. Maimone, L. Celona, and F. Chines, "Status of the versatile ion source VIS", in *Proc. EPAC'08*, Genoa, Italy, 2008, paper MOPC151. https://jacow.org/e08/papers/mopc151.pdf

[14] Valley Design Corp., https://valleydesign.com/

[15] D.M. Pozar, *Microwave Engineering*, 4th ed., New York, NY, USA: Wiley, 2011.

[16] N. Marcuvitz, *Waveguide Handbook*, MIT Radiation Laboratory Series, New York, NY, USA: McGraw-Hill, 1986, pp. 223-224.

[17] Ansys HFSS, https://www.ansys.com/products/electronics/ansys-hfss